IEIE Transactions on Smart Processing and Computing, vol. 4, no. 2, April 2015
http://dx.doi.org/10.5573/IEIESPC.2015.4.2.097

Strong Uncorrelated Transform Applied to Spatially Distant Channel EEG Data

Youngjoo Kim and Cheolsoo Park

Department of Computer Engineering, Kwangwoon University / Seoul, Korea
{lyoungjookiml@gmail.com, parkcheolsoo@kw.ac.kr}

***** Corresponding Author: Cheolsoo Park

Received November 20, 2014; Revised December 27, 2014; Accepted February 12, 2015; Published April 30, 2015

** Short Paper*

***Abstract*:** In this paper, an extension of the standard common spatial pattern (CSP) algorithm using the strong uncorrelated transform (SUT) is used in order to extract the features for an accurate classification of the left- and right-hand motor imagery tasks. The algorithm is designed to analyze the complex data, which can preserve the additional information of the relationship between the two electroencephalogram (EEG) data from distant channels. This is based on the fact that distant regions of the brain are spatially distributed spatially and related, as in a network. The real-world left- and right-hand motor imagery EEG data was acquired through the Physionet database and the support vector machine (SVM) was used as a classifier to test the proposed method. The results showed that extracting the features of the pair-wise channel data using the strong uncorrelated transform complex common spatial pattern (SUTCCSP) provides a higher classification rate compared to the standard CSP algorithm.

***Keywords*:** CSP, SUTCCSP, MEMD, Complex, Motor imagery

1. Introduction

Brain computer interface (BCI) technology offers the people the ability to control, connect and respond to a given environment. This technology is being used in various fields including rehabilitation, education and entertainment [1-3]. For example, one of the most popular BCI trends allow people to control electronic devices without moving their arms. Patients who suffer from local or muscle paralysis are also capable of controlling the environment under such harsh conditions merely by imagining the state of moving certain body parts. Thus, recent studies have focused on the so-called 'motor imagery' of the left- and right-hand [4-8] or finger movement [9]. Since an accurate classification of different motor imagery tasks is required for this environmental control and communication through the motor imagery electroencephalogram (EEG) data, extracting the optimal features from the data is the cornerstone for classification.

Feature extraction methods can be divided into two methods: an unsupervised learning method and a supervised learning method, which unlike the former method, requires a priori information. Among the most frequently used unsupervised statistical methods, principal component analysis (PCA) and independent component analysis (ICA) are commonly used. A. Vallabhaneni et al. applied PCA to extract the features of motor imagery tasks and use them on both spatial and temporal dimensions [7]. C. Brunner et al. applied PCA in order to reduce the number of components and used three different ICA algorithms in order to find the optimal spatial filter that increases the single trial classification rate [10].

For a supervised statistical method, the common spatial pattern (CSP) [11] is well used based on the fact that spatially allocated regions of the brain are activated when performing such motor imagery tasks [8]. The CSP algorithm maximizes the variance-ratio of two classes, so that the variance information of the two classes is used in order to improve the distinction between the two.

Furthermore, many extensions to the standard CSP algorithm are also being studied with the aim of finding and using additional statistical information of the data for better classification. An analytic signal-based CSP (ACSP) algorithm was first proposed by O. Falzon et al. [12], which uses the Hilbert transform and an analytical representation. In particular, a complex form of EEG

signals is used in order to better distinguish different mental tasks.

Recently, an augmented complex common spatial pattern (ACCSP) combined with the strong uncorrelated transform was proposed to analyze the motor imagery EEG data by pairing the adjacent channels [13]. This pair-wise approach uses additional information based on the fact that adjacently allocated channels are activated in relation to each other when performing motor imagery tasks. On the other hand, although there are more network connections in the adjacent channels compared to the distant channels, the distant channels still have interactions between them and are related so as to form a network.

In this paper, the distant channels are paired into a complex form and their variance information are used as features. The features acquired using the proposed algorithm includes additional information of the relationship of every two channels, based on the fact that distant channels are related inside the brain network. The multivariate extension of the empirical mode decomposition (MEMD) is used instead of infinite impulse response (IIR) band-pass filtering methods to gain the 8-25 Hz frequency band for the motor imagery EEG data. Next, the features are extracted using the strong uncorrelated transform complex common spatial pattern (SUTCCSP), which conclusively hold additional information of the power difference between the distant channels. An SVM classifier that uses a Gaussian kernel function then evaluates the performance of the proposed algorithm and a series of experiments with real-world data shows that the SUTCCSP results in a higher classification rate compared to the original CSP algorithm by 1.5%.

2. Methods

The motor imagery EEG data used to test the performance of the proposed algorithm is acquired from the Physiobank Motor/Mental Imagery (MMI) database, Physionet[1] [15]. A total of 45 trials for the left- and right-hand motor imagery tasks are each recorded for 109 subjects. Specifically, in this paper, 20 subjects starting from the last subject are chosen to evaluate the proposed algorithm. Among all the channels that cover the scalp regions, six channels in Fig. 1 are chosen to test the proposed algorithm. In particular, the six distant regions include the distant channels of the cortex area, where the neural activities of motor imagery are concentrated. The sampling frequency of the recorded data is 160 Hz, producing a total of 640 samples for each trial.

2.1 Preprocessing

MEMD is an alternative preprocessing method of gaining the 8-25 Hz frequency band. MEMD is a fully data-driven time-frequency analysis for non-linear and non-stationary multichannel bio-signal data [16]. The given data is decomposed into several intrinsic mode functions (IMFs) and each IMF covers a particular frequency band. Fig. 2 shows a periodogram (Bartlett window) [17] that represents the power spectra of each IMF and shows the averaged data of all the trials of 20 subjects. As shown in Fig. 2, the third and fourth IMFs correspond to the beta (14-20 Hz) and mu (8-12 Hz) rhythms, respectively. Since they cover the 8-25 Hz frequency band, the third and fourth IMFs are added in order to produce a preprocessed signal containing the 8-25 Hz frequency components. Table 1 lists the specific steps for the MEMD algorithm [16]. If an ordinary sphere is extended to an arbitrary dimension, it is defined as an n sphere and an n sphere belongs to an (n+1)-dimensional Euclidean coordinate system, as mentioned in [16]. The direction vectors **x** of an n-dimensional space are the signal projections and are denoted as points on an (n-1) sphere.

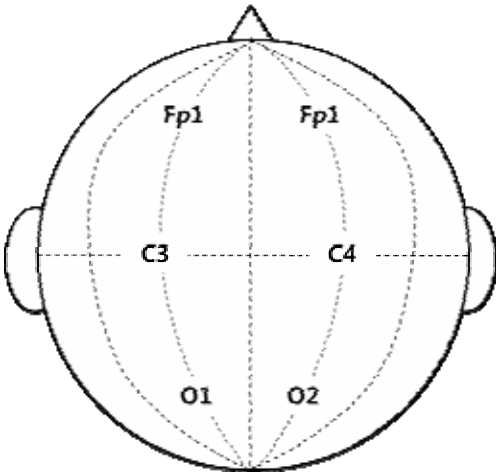

Fig. 1. EEG montage of the selected six channels. All combinations of choosing two channels out of 6 are used as complex forms. Therefore, a total of 15 paired channel data are applied when extracting the features.

2.2 Strong Uncorrelated Transform Common Spatial Pattern

The combination of choosing two out of six channels, as illustrated in Fig. 1, are used to form distinct 15 complex random variable vectors, which can be generally defined as, $\mathbb{Z} = \mathbf{z}_r + j\mathbf{z}_i$. Each data of one channel is paired with another to form a complex form as $\mathbb{Z}$. The covariance and pseudocovariance is calculated as follows [18]:

$$\begin{aligned}\mathbf{C} &= E\left[\mathbb{Z}\mathbb{Z}^H\right] \quad \#\\ &= E\left[\left(\mathbf{z}_r + j\mathbf{z}_i\right)\left(\mathbf{z}_r - j\mathbf{z}_i\right)^T\right] \quad (1)\\ &= E\left[\mathbf{z}_r\mathbf{z}_r^T + \mathbf{z}_i\mathbf{z}_i^T\right] + jE\left[\mathbf{z}_i\mathbf{z}_r^T + \mathbf{z}_r\mathbf{z}_i^T\right] \geq 0 \ \#\\ \mathbf{P} &= E\left[\mathbb{Z}\mathbb{Z}^T\right]\\ &= E\left[\left(\mathbf{z}_r + j\mathbf{z}_i\right)\left(\mathbf{z}_r + j\mathbf{z}_i\right)^T\right] \quad (2)\\ &= E\left[\mathbf{z}_r\mathbf{z}_r^T\right] - E\left[\mathbf{z}_i\mathbf{z}_i^T\right] + jE\left[\mathbf{z}_i\mathbf{z}_r^T + \mathbf{z}_r\mathbf{z}_i^T\right]\end{aligned}$$

[1] www.bci2000.org

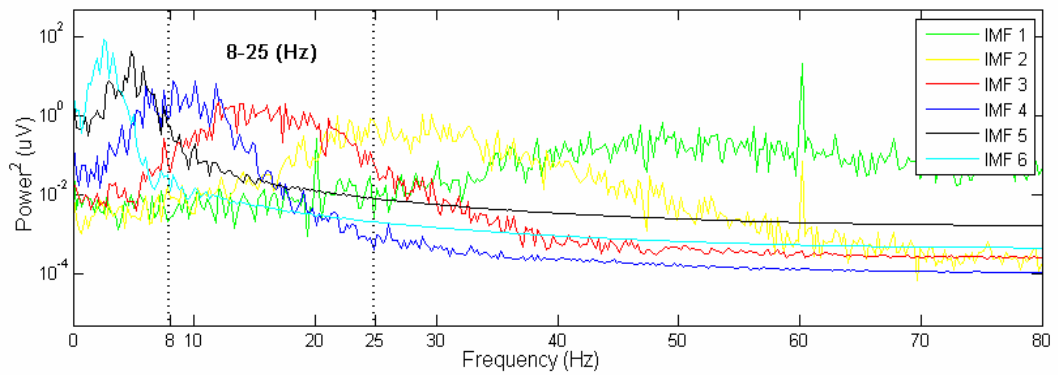

Fig. 2. Power spectra of the first 6 IMFs. 'IMF 3' and 'IMF 4' covers the 8-25 Hz frequency band. The peak in 60 Hz is the power noise.

Table 1. MEMD algorithm.

1. Choose a suitable point set for sampling on an (n-1) sphere.
2. Calculate a projection, denoted by $\{p^{\theta_k}(t)\}_{t=1}^{T}$, of the input signal $\{\mathbf{v}(t)\}_{t=1}^{T}$ along the direction vector $\mathbf{x}^{\theta_k}$, for all k (the whole set of direction vectors), giving $\{p^{\theta_k}(t)\}_{t=1}^{K}$ as the set of projections.
3. Find the time instants $t_j^{\theta_k}$ corresponding to the maxima of the set of projected signals $\{p^{\theta_k}(t)\}_{t=1}^{K}$.
4. Interpolate $[t_j^{\theta_k}, \mathbf{v}(t_j^{\theta_k})]$ to obtain multivariate envelop curves $\{e^{\theta_k}(t)\}_{t=1}^{K}$.
5. For a set of K direction vectors, the mean $\mathbf{m}(t)$ of the envelop curves is calculated as $\mathbf{m}(t) = 1/K \sum_{k=1}^{K} e^{\theta_k}(t)$.
6. Extract the "detail" $\mathbf{c}_i(t)$ using $\mathbf{c}_i(t) = \mathbf{v}(t) - \boldsymbol{m}(t)$ (I is an order of IMF). If the "detail" $\mathbf{c}_i(t)$ fulfills the stoppage criterion for a multivariate IMF, apply the above procedure to $\mathbf{v}(t) - \mathbf{c}_i(t)$, otherwise apply it to $\mathbf{c}_i(t)$.

where $E[\cdot]$ is the statistical expectation operator and $(\cdot)^H$ and $(\cdot)^T$ each indicate the Hermitian and transpose of the data, respectively. If the data is circular, $\boldsymbol{z}_r$ and $\boldsymbol{z}_i$ become uncorrelated, so that Eq. (2) equals to zero. On the other hand, due to the non-circularity of the real-world signals [19], the pseudocovariance information can be preserved when the augmented complex CSP is applied [13]. Additionally, when SUT is applied, the multichannel complex data becomes uncorrelated. The procedures for extracting the features and finding the spatial filtered data using SUTCCSP are explained as follows:

$$\begin{cases} \mathbf{C}_1 = E\left[\mathbf{A}_1\mathbf{A}_1^H\right] \\ \mathbf{C}_2 = E\left[\mathbf{A}_2\mathbf{A}_2^H\right] \end{cases} \tag{3}$$

$$\begin{cases} \mathbf{P}_1 = E\left[\mathbf{A}_1\mathbf{A}_1^T\right] \\ \mathbf{P}_2 = E\left[\mathbf{A}_2\mathbf{A}_2^T\right] \end{cases} \tag{4}$$

where $\mathbf{A}_1$ and $\mathbf{A}_2$ are the $N \times S$ matrices when $\mathbf{S}$ is the sample size and $\mathrm{N} = \binom{6}{2}$ since every possible combination of choosing two out of a six channel data, each becomes a complex data yielding a total of 15 combinations in this paper. $\mathbf{C}_{1\,or\,2}$ is the covariance matrices and $\mathbf{P}_{1\,or\,2}$ is the pseudocovariance matrices when $\mathbf{A}_1$ and $\mathbf{A}_2$ corresponds to the left- and right-hand class data, respectively. The composite form matrices are defined as

$$\begin{cases} \mathbf{C}_c = \mathbf{C}_1 + \mathbf{C}_2 = E\left[\mathbf{A}_1\mathbf{A}_1^H\right] + E\left[\mathbf{A}_1\mathbf{A}_1^H\right] \\ \mathbf{P}_c = \mathbf{P}_1 + \mathbf{P}_2 = E\left[\mathbf{A}_1\mathbf{A}_1^T\right] + E\left[\mathbf{A}_2\mathbf{A}_2^T\right] \end{cases} \tag{5}$$

When the eigenvalue decomposition is applied, Eq. (6) is whitened by a whitening matrix $\mathbf{G} = \boldsymbol{\Lambda}_c^{-1/2}\mathbf{U}_c^H$ and $\mathbf{G}\mathbf{C}_c\mathbf{G}^H$ is equivalent to the identity matrix ($\mathbf{I}$). Therefore, the pseudocovariance matrix is decomposed with Takagi's factorization, as shown in Eq. (7).

$$\mathbf{C}_c = \mathbf{U}_c\boldsymbol{\Lambda}_c\mathbf{U}_c^H \tag{6}$$

$$\mathbf{P}_c = \mathbf{G}\mathbf{P}_c\mathbf{G}^T = \mathbf{Y}\boldsymbol{\Lambda}\mathbf{Y}^T \tag{7}$$

Then the SUT matrix is calculated as Eq. (8), which diagonalizes the covariance and pseudocovariance matrices simultaneously, as shown in Eq. (9).

$$\mathbf{Q} = \mathbf{Y}^H\boldsymbol{G} \tag{8}$$

$$\begin{cases} \mathbf{Q}\mathbf{C}_C\mathbf{Q}^H = \mathbf{Q}\mathbf{C}_1\mathbf{Q}^H + \mathbf{Q}\mathbf{C}_2\mathbf{Q}^H = \mathbf{I} \\ \mathbf{Q}\mathbf{P}_C\mathbf{Q}^H = \mathbf{Q}\mathbf{C}_1\mathbf{Q}^T + \mathbf{Q}\mathbf{C}_2\mathbf{Q}^T = \boldsymbol{\Lambda} \end{cases} \tag{9}$$

When $\mathbf{S}_1 = \mathbf{Q}\mathbf{C}_1\mathbf{Q}^H$ and $\mathbf{S}_2 = \mathbf{Q}\mathbf{C}_2\mathbf{Q}^H$ is defined, the

covariance matrix is estimated as below:

$$\begin{cases} \mathbf{\Lambda}_1 = \mathbf{B}^{-1}\mathbf{S}_1\mathbf{B} \\ \mathbf{\Lambda}_2 = \mathbf{B}^{-1}\mathbf{S}_2\mathbf{B} \end{cases} \quad (10)$$

Additionally, the eigenvectors of the estimation of the pseudocovariance can also be derived using $\hat{\mathbf{Q}} = \mathbf{\Lambda}^{-1/2}\mathbf{Y}^H\mathbf{G}$, as in Eq. (13), where $\hat{\mathbf{B}}$ and $\hat{\mathbf{\Lambda}}_{1or}$ correspond to the eigenvectors and eigenvalues of $\hat{\mathbf{S}}_{1and}$, respectively.

$$\begin{cases} \hat{\mathbf{S}}_1 = \hat{\mathbf{Q}}\mathbf{P}_1\hat{\mathbf{Q}}^T \\ \hat{\mathbf{S}}_2 = \hat{\mathbf{Q}}\mathbf{P}_2\hat{\mathbf{Q}}^T \end{cases} \quad (11)$$

$$\hat{\mathbf{S}}_1 + \hat{\mathbf{S}}_2 = \mathbf{I} \quad (12)$$

$$\begin{cases} \hat{\mathbf{B}}^{-1}\hat{\mathbf{S}}_1\hat{\mathbf{B}} = \hat{\mathbf{\Lambda}}_1 \\ \hat{\mathbf{B}}^{-1}\hat{\mathbf{S}}_2\hat{\mathbf{B}} = \hat{\mathbf{\Lambda}}_2 \end{cases} \quad (13)$$

Eqs. (12) and (16) show that the variance–ratio between two classes is maximized.

$$\begin{cases} \mathbf{W} = \mathbf{B}^{-1}\mathbf{G} \\ \hat{\mathbf{W}} = \hat{\mathbf{B}}^{-1}\hat{\mathbf{G}} \end{cases} \quad (14)$$

Thus, the spatial filters of Eq. (14) are applied to the original data A, as shown below:

$$\begin{cases} \mathbf{V} = \mathbf{W}\mathbf{A} \\ \hat{\mathbf{V}} = \hat{\mathbf{W}}\mathbf{A} \end{cases} \quad (15)$$

where $\mathbf{V}$ and $\hat{\mathbf{V}}$ are the final spatial filtered data using the covariance and pseudocovariance matrices, respectively. These extracted features are then used in SVM, which uses a Gaussian kernel and the left- and right-hand motor imagery tasks are classified.

2.3 Performance Evaluation

In this paper, both the CSP algorithm, which takes into account the power difference information of the two distant channel data as additional features, was used to test the performance of SUTCCSP. Additionally, the ACCSP based method was used to compare with SUTCCSP. Without SUT, the ACCSP based method cannot preserve the pseudocovariance information since the pseudocovariance information is lost during the whitening process. Moreover, the remaining covariance information only contains the sum of the power of complex signals, thus, a lower performance compared to SUTCCSP and CSP is expected in this case.

For performance evaluation, the same data was classified using SVM repeatedly for 40 times, in order to obtain an average classification rate. Among the 20 subjects, subjects are chosen as significant when the classification rates are above 64% (confidence limit = 95%) [20].

Table 2. Classification rates of CSP and SUTCCSP.

	CSP	ACCSP	SUTCCSP
Classification Rate (%)	69.78	68.89	71.28

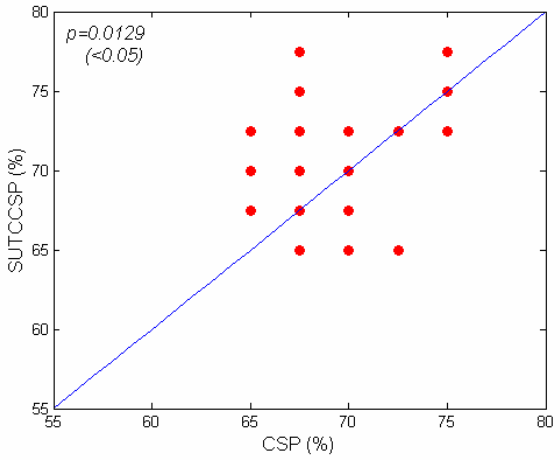

Fig. 3. Scatter-plot of the classification rate of SUTCCSP and the original CSP. The improved performance is shown using the *p*-value (*p*=0.0129) of the t-test.

The average CSP, ACCSP and SUTCCSP classification rates of the subjects who are chosen as significant in both CSP, ACCSP and SUTCCSP throughout the 40 repetitions using SVM, are compared in Table. 2. As shown in Table 2, SUTCCSP produces a higher separation rate compared to the standard CSP algorithm and the ACCSP based method also produces a lower performance compared to the performance of SUTCCSP, as expected.

Fig. 3 shows the performance comparison between SUTCCSP and CSP. For every test, out of a total of 40 trials using SVM, all the significant subjects are displayed in Fig. 3 The paired sample t-test for CSP and SUTCCSP was used in order to test the performance enhancement of SUTCCSP. The t-test is applied to the 40 CSP average classification rates and the other 40 SUTCCSP classification rates gained each from the 40 trials using SVM. As a result, the t-test yields a *p*-value of 0.0129 (<0.05), which is small enough to reject the null hypothesis, thus proving the enhanced performance of SUTCCSP compared to the standard CSP algorithm.

3. Conclusion

MEMD was used for preprocessing in order to analyze the frequency. A complex form of pairing spatially distant channel EEG data was analyzed using SUTCCSP in order to use the power difference information as features. This assumes that spatially distant regions of the brain are connected and are related to one another as a network. Results show that SUTCCSP applied to the complex forms of spatially distant channel data yields an enhanced

classification rate compared to the original CSP algorithm.

Acknowledgement

This research is supported by the Basic Science Research Program through the National Research Foundation of Korea (NRF) funded by the Ministry of Education, Science and Technology (2014R1A1A2059483)

References

[1] B. Graimann, G. Pfurtscheller, and B. Allison, "Brain-Computer Interfaces," Springer-Verlag Berlin Heidelberg, 2010. Article (CrossRef Link)

[2] B. Blankertz, G. Dornhege, M. Krauledat, K. Mueller, and G. Curio, " The non-invasive Berlin Brain-Computer Interface: fast acquisition of effective performance in untrained subjects," NeuroImage, vol. 37, no. 2, pp. 539-550, 2007. Article (CrossRef Link)

[3] G. Pfurtscheller, G.R. M¨uller-Putz, A. Schl¨ogl, B. Graimann, R. Scherer, R. Leeb, C. Brunner, C. Keinrath, F. Lee, G. Townsend, C. Vidaurre, C. Neuper, "15 years of BCI research at Graz University of technology: current projects," IEEE Transactions on Neural Systems and Rehabilitation Engineering, vol. 14, no. 2, 2006, pp. 205-210, 2006. Article (CrossRef Link)

[4] A. Vallabhaneni and B. He, "Motor imagery task classification for brain computer interface applications using spatiotemporal principle component analysis," Neurological Research, vol. 26, no. 3, pp. 282-287, 2004. Article (CrossRef Link)

[5] X. Guo and X. Wu, "Motor imagery EEG classification based on dynamic ICA mixing matrix," Bioinformatics and Biomedical Engineering (iCBBE), 4th International Conference, 2010. Article (CrossRef Link)

[6] C.R. Hema, M.P. Paulraj, S. Yaacob, A.H. Adom, and R. Nagarajan, " Motor imagery signal classification for a four state brain machine interface," International Journal of Computer, Information, Systems and Control Engineering, vol. 1, no. 5, pp. 1360-1365, 2007. Article (CrossRef Link)

[7] A. Vallabhaneni and B. He, "Motor imagery task classification for brain computer interface applications using spatiotemporal principle component analysis," Neurological Research, vol. 26, no. 3, pp. 282-287, 2004. Article (CrossRef Link)

[8] H. Ramoser, J. Muller-Gerking, and G. Pfurtscheller, "Optimal spatial filtering of single trial EEG during imagined hand movement," IEEE Trans. Rehabil. Eng., vol. 8, no. 4, pp. 441–446, 2000. Article (CrossRef Link)

[9] C.I. Hung, P.L. Lee, Y.T. Wu, L.F. Chen, T.C. Yeh, and J.C. Hsieh, " Recognition of motor imagery electroencephalography using independent component analysis and machine classifiers," Annals of Biomedical Engineering, vol. 33, no. 8, pp. 1053-1070, 2005. Article (CrossRef Link)

[10] C. Brunner, M. Naeem, R. Leeb, B. Graimann, and G. Pfurtscheller, "Spatial filtering and selection of optimized components in four class motor imagery EEG data using independent components analysis, " Pattern Recognition Letters, vol. 28, no. 8, pp. 957-964, 2007. Article (CrossRef Link)

[11] Z.J. Koles, "The quantitative extraction and topographic mapping of the abnormal components in the clinical EEG," Electroenceph. Clin. Neurophysiol., vol. 79, no. 6, pp. 440–447, 1991. Article (CrossRef Link)

[12] O. Falzon, K.P. Camilleri, and J. Muscat, "Complex-valued spatial filters for task discrimination," Proceedings of International Conference of the IEEE Engineering in Medicine and Biology Society (EMBC), pp. 4707-4710, 2010. Article (CrossRef Link)

[13] C. Park, Clive C. Cheong-Took, and D. P. Mandic, "Augmented complex common spatial patterns for classification of noncircular EEG from motor imagery tasks," IEEE Transactions on Neural Systems and Rehabilitation Engineering, vol. 22, no. 1, pp. 1-10, 2014. Article (CrossRef Link)

[14] E. Urrestarazu, P. LeVan, and J. Gotman, "Independent component analysis identifies ictal bitemporal activity in intracranial recordings at the time of unilateral discharges," Clin. Neurophysiol., vol. 117, pp.549-561 2006. Article (CrossRef Link)

[15] A. L. Goldberger, L. A. N. Amaral, L. Glass, J. M. Hausdorff, P. Ch. Ivanov, R. G. Mark, J. E. Mietus, G. B. Moody, C. Peng, and H. E. Stanley, "PhysioBank, PhysioToolkit, and PhysioNet: Components of a New Research Resource for Complex Physiologic Signals," Circulation, vol. 101, no.23, pp. 215-220, 2000. Article (CrossRef Link)

[16] N. Rehman and D. P. Mandic, "Multivariate empirical mode decomposition," Proceedings of the Royal Society A, vol. 466, pp. 2117, pp. 1291 -1302, 2010. Article (CrossRef Link)

[17] P. Stoica and R. L. Moses, "Introduction to spectral analysis," New Jersey: Prentice Hall, vol. 1. 1997. Article (CrossRef Link)

[18] J. Navarro-Moreno , M. D. Estudillo-Martinez , R. M. Fernandex-Alcala and J. C. Ruiz-Molina, "Estimation of improper complex valued random signals in colored noise by using the Hilbert space theory", IEEE Trans. Inf. Theory, vol. 55, no. 6, pp. 2859 - 2867, 2009. Article (CrossRef Link)

[19] D. P. Mandic and S.L. Goh, "Complex Valued Nonlinear Adaptive Filters," Hoboken, NJ: Wiley, 2009. Article (CrossRef Link)

[20] G. R. M¨uller-Putz, R. Scherer, C. Brunner, R. Leeb, and G. Pfurtscheller, "Better than random? A closer look on BCI results," International Journal of Bioelectromagnetism, vol. 10, no. 1, pp. 5255, 2008. Article (CrossRef Link)

Youngjoo Kim received her B.S. degree in Computer Engineering from Kwangwoon University, Seoul, South Korea, in 2015. Currently, she is a graduate student in the Bio-Medical Computing Laboratory (BMCL), Department of Computer Engineering, Kwangwoon University, Seoul, South Korea. Her research interests include bio-medical signal processing, machine learning and statistical analysis.

Cheolsoo Park is an assistant professor of Computer Engineering at Kwangwoon university, Seoul, South Korea. He received the B. Eng. degree in electrical engineering from Sogang University, Seoul, South Korea, and the M. Sc. degree in biomedical engineering department from Seoul National University, Seoul, South Korea. In 2012, he received his PhD degree in adaptive nonlinear signal processing from Imperial College London, London, U.K and worked as a postdoctoral researcher in bioengineering department at University California, San Diego, U.S. His research interests are mainly in the area of machine learning, adaptive and statistical signal processing, with applications in brain computer interface, computational neuroscience and wearable technology. He is a member of the IEEE.